Chinese Journal of
POLYMER SCIENCE

RESEARCH ARTICLE

https://doi.org/10.1007/s10118-026-3766-7
Chinese J. Polym. Sci.

Moisture-resistant and Thermally Dual-detachable Silicone-contained Pressure-sensitive Adhesive: Preparation and Potential Applications in Medical Care

Feng-Ming Yin[a,†], Xiao-Xia Zhou[a,†], Hai-Chao Yu[c], Shu-Sheng Li[a,b*], Zhi-Qiu Ye[a], Xu-Bao Jiang[a], Xiao-Li Zhu[a*], Sheng-Yu Feng[b], and Xiang-Zheng Kong[a]

[a] *Shandong Provincial Key Laboratory of Extreme Environment-tolerant Specialty Chemicals, College of Chemistry and Chemical Engineering, University of Jinan, Jinan 250022, China*
[b] *National Engineering Research Center for Colloidal Materials & Key Laboratory of Special Functional Aggregated Materials, Ministry of Education; School of Chemistry and Chemical Engineering, Shandong University, Jinan 250100, China*
[c] *Department of Orthopaedics, Qilu Hospital, Cheeloo College of Medicine, Shandong University, Jinan 250012, China*

Electronic Supplementary Information

Abstract Thermo-responsive pressure-sensitive adhesives (PSAs) offer significant potential for advanced wound care but face challenges in achieving simultaneously robust physiological adhesion and controllable, atraumatic removal. This study introduces silicone-contained pressure-sensitive adhesive (SiPSA), the adhesive platform synthesized by crosslinking thermo-responsive poly(ethylene glycol-*co*-siloxane) (PEG-Si) with trimethylol-propane triacrylate and chitosan tackifier. SiPSA exhibits dual-temperature-triggered debonding, delivering exceptional adhesion on skin at 37 °C (180° peel strength=211 N/m), while enabling rapid, on-demand detachment *via* either heating to 60 °C (72.7% adhesion reduction) or cooling to 0 °C (82.5% adhesion reduction). Critically, SiPSA maintains robust interfacial bonding under high-humidity conditions, adhering effectively to moist skin and bleeding wounds, and retaining significant peel strength even after absorbing 20 vol% water, a key advantage for exudative wound management and aqueous environments. Comprehensive biocompatibility tests confirmed its non-irritating and clinically safe profile. Compared to conventional dressings, SiPSA uniquely integrates high-strength physiological adhesion with programmable, painless removal through distinct thermal stimuli, significantly enhancing patient comfort and clinical utility. These results highlight SiPSA as an advanced material for medical care, providing reliable adhesion modulation, excellent performance in wet settings, and favorable patient compliance.

Keywords Thermally dual-detachable; Pressure sensitive adhesive; Moisture-resistant; Medical care

Citation: Yin, F. M.; Zhou, X. X.; Yu, H. C.; Li, S. S.; Ye, Z. Q.; Jiang, X. B.; Zhu, X. L.; Feng, S. Y.; Kong, X. Z. Moisture-resistant and thermally dual-detachable silicone-contained pressure-sensitive adhesive: preparation and potential applications in medical care. *Chinese J. Polym. Sci.* https://doi.org/10.1007/s10118-026-3766-7

INTRODUCTION

Medical pressure-sensitive adhesives (PSAs) are vital for diverse epidermal applications including medical tapes, wound dressings, catheter securement devices, and biosensing patches.[1–5] While outperforming traditional materials in terms of convenience, safety, and aesthetics,[6–9] current medical PSAs face critical limitations such as compromised biocompatibility, humidity-induced adhesion failure, and significant risk of secondary injury upon removal.[2,10,11]

Thermally debonding PSAs offer a promising strategy for mitigating removal trauma. These stimuli-responsive systems maintain strong interfacial adhesion at physiological temperatures, but undergo programmable detachment upon specific thermal triggers (heating or cooling).[12–16] For example, Hwang *et al*.[15] developed a thermo switchable PSA by copolymerizing *N*-isopropylacrylamide, acrylic acid, and 2-ethylhexyl acrylate, achieving release at 80 °C. Conversely, Zeng *et al*.[16] engineered a low-temperature debondable PSA exploits the phase transition of semicrystalline-to-amorphous at 26 °C. Crucially, the debonding temperature must be precisely tuned: excessive heat risks tissue damage, while temperature near ambient conditions undermine adhesion stability and utility.

Polysiloxanes are renowned for their exceptional biocompatibility, thermal stability, and non-toxicity in biomedical contexts,[17–22] underpin a rapidly growing class of silicone-contained PSAs (SiPSA). Their intrinsic inertness minimizes their interference with wound healing.[1,23–29] However, conventional SiPSAs exhibit two persistent drawbacks: (1) inher-

* Corresponding authors, E-mail: chm_liss@ujn.edu.cn (S.S.L.)
E-mail: chm_zhuxl@ujn.edu.cn (X.L.Z.)
† These authors contributed equally to this work.
Received April 20, 2026; Accepted June 1, 2026; Published online September 20, 2026

ent hydrophobicity leading to adhesion failure in moist wound environments, and (2) insufficient adhesive strength for exuding or open wounds.[30]

We have previously synthesized poly(ethylene glycol-*co*-siloxane) (PEG-Si) through the aza-Michael addition of polyethylene glycol diacrylate (PEGDA) and 1,3-bis(3-amino-propyl)-1,1,3,3-tetramethyldisiloxane.[31] The resulting material showed excellent biocompatibility and temperature-dependent hydrophilic-hydrophobic transition. Building on this work, we introduce a thermosensitive SiPSA. SiPSA uniquely integrates trimethylolpropane triacrylate (TMPTA) as a crosslinker and chitosan as a tackifier within the PEG-Si network (Fig. 1a). The key innovation lies in its dual thermal switching mechanism: crystalline PEGDA domains enable clean low-temperature debonding, whereas the LCST-type PEG-Si backbone facilitates high-temperature release (Fig. 1b). Remarkably, SiPSA maintained robust adhesion even on hydrated skin, tolerating moisture uptake exceeding 20 vol% without significant performance loss (Fig. 1c). This study systematically evaluated the thermo-responsiveness, water uptake, degradability, and biocompatibility of SiPSA, establishing it as a versatile platform for wound management, emergency hemostasis, and biosensing applications demanding high adhesion strength, safe on-demand detachment, and moisture tolerance (Fig. 1d).

EXPERIMENTAL

Materials

Poly(ethylene glycol diacrylate) (PEGDA, 99%, M_n=600 g/mol), trimethylolpropane triacrylate (TMPTA, 99%), chitosan (degree of deacetylation ≥95%, M_w=5×10^4–6×10^4 g/mol) diiodomethane (CH_2I_2, 99%), trifluoroacetic acid (TFA, 99%), ammonium acetate (NH_4OAc, 99%), diclofenac sodium (DFS, 99%), and poly(ethylene glycol) (PEG, 99%, M_n=400 g/mol) were purchased from Aladdin (Shanghai). 1,3-Bis(3-amino-propyl)-1,1,3,3-tetra-methyldisiloxane (APDS, 99%) was purchased from Xinmingtai Chemicals (Hubei, China). Dichloromethane (CH_2Cl_2, 99%) and glacial acetic acid (99%) were supplied by Fuyu Chemical (Tianjin). Lysine polypeptide (98%) and cysteine polypeptide (98%) were obtained from Cellmano Biotech (Hefei, China). PVC, SUS303 stainless steel, PP, and PE sheets, along with PET release film, were acquired from Hokuto (Guangdong).

Synthesis of PEG-Si

PEG-Si was synthesized *via* catalyst-free aza-Michael addition between APDS and PEGDA according to our previously reported protocol.[31] Briefly, APDS (2.49 g, 10 mmol) and PEGDA (5.75 g, 10 mmol) were co-dissolved in CH_2Cl_2 (50 mL) and stirred magnetically at 25 °C for 24 h (monitored by Fourier transform infrared (FTIR) spectroscopy for complete acrylate group conversion). The reaction mixture was concentrated by rotary evaporation, yielding PEG-Si as a colorless, hygroscopic viscous liquid (yield: 96%).

Preparation of SiPSA

SiPSA was obtained by blending PEG-Si with varying concentrations of TMPTA (0.25 wt%–1.75 wt%) and a preformed chitosan solution. The chitosan solution was prepared by dissolving 1 g of chitosan powder in 10 g of deionized water, followed by pH adjustment to 6.5 using glacial acetic acid, yielding a pale-yellow viscous solution. The mixture was homogenized under stirring to ensure uniformity, and then coated onto a release film using a four-side applicator. The films were cured at 30 °C for 3 h, then SiPSA-T_x-C_y was produced, where *x* and *y* denote the mass fraction of TMPTA (wt%) and chitosan (wt%), respectively.

Structural and Thermal Properties Characterization

The chemical structure of PEG-Si was characterized by nuclear magnetic resonance (NMR, Advance III, 400 MHz, D_2O as solvent, Brüker, USA) and Fourier transform infrared spectroscopy (FTIR, Tensor 27, Brüker, USA) using the KBr pellet method in a scan range of 4000–400 cm^{-1}. Thermal properties were evaluated by differential scanning calorimetry (DSC, DSC25, TA Instrument, USA) at N_2 atmosphere in the temperature range from

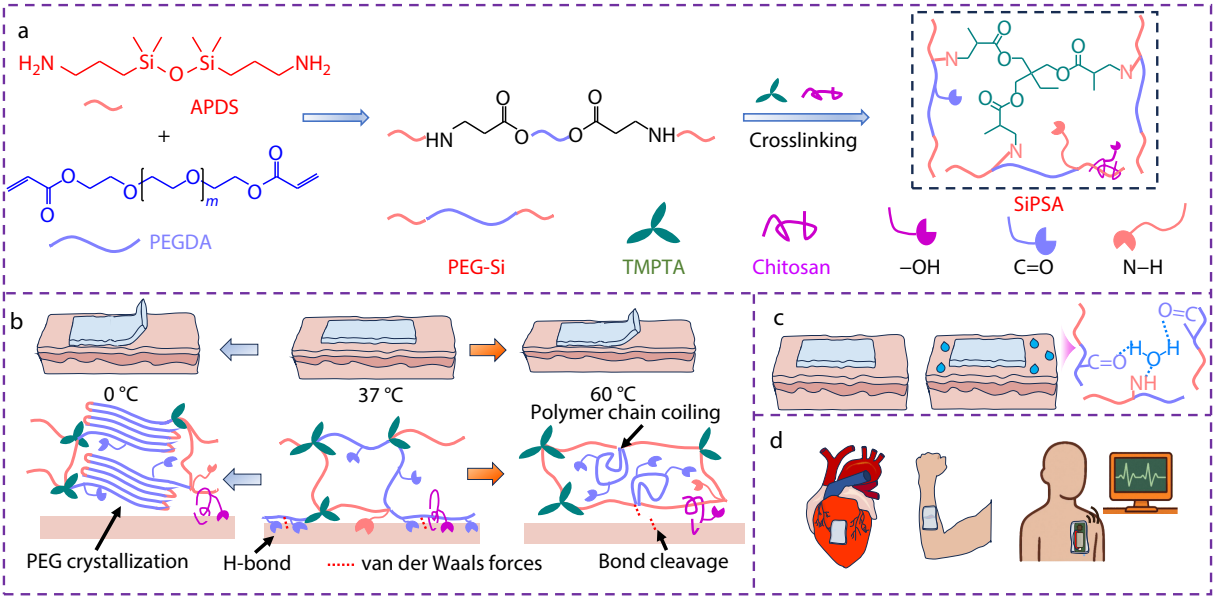

Fig. 1 (a) Structure schematic diagram of SiPSA and (b) its high-/low-temperature debonding mechanism; (c) Adhesion to wet skin and (d) application for wound dressings and biosensing patches.

−80 °C to 80 °C at heating rate 10 °C/min to determine the glass transition temperature (T_g). The changes in the crystallinity of the samples were characterized by X-ray diffraction (XRD, D8 FOCUS, Brüker, USA) over a 2θ range of 5°–80° at a scanning rate of 6 (°)/min. Thermogravimetric analysis (TGA, TGA55, TA Instruments, USA) was performed at N_2 atmosphere over the temperature range of 30–600 °C at heating rate 10 °C/min. Additionally, viscoelasticity properties were analyzed using a rotational rheometer (HR20, TA Instruments, USA) over the temperature range from −50 °C to 65 °C to measure the storage modulus (E') and loss modulus (E'').

Adhesion Performance Testing

180° Peel strength

180° Peel strength (N/m) was determined according to GB/T 2792-2014 using a universal tensile tester (HD-B609B-S, Haida Instrument, China). Rectangular SiPSA-T_x-C_y films (25 mm × 100 mm) were laminated onto PET, PP, PE, PVC, SUS303 stainless steel, and skin substrates using a 2.5 kg hand-roller (10 mm/s, 3 passes). The bonded assembly was peeled at a rate of 300 mm/min at 180°, and the steady-state peel force normalized to the film width was recorded.

Hold tack (h)

The holding time to failure was assessed by adhering a SiPSA-T_x-C_y film (25.0 mm × 75.0 mm × 0.1 mm) between two steel plates (25 mm × 25 mm overlap) and subjecting the assembly to a 1 kg suspended weight.

Probe tack

Probe tack (N) was quantified using a probe-tack testing machine (TC-HCN02, Taichang Instruments, China), with a 10.0 mm × 10.0 mm × 0.1 mm specimen at a retraction rate of 1 mm/min, and the peak detachment force was recorded as the tack strength. The probe displacement (x) and the load force ($F(x)$) were measured. The work of adhesion (W, J/m^2) was calculated using Eq. (1):[32,33]

$$W = \frac{1}{A}\int_{x_0}^{x_1} F(x)\mathrm{d}x \tag{1}$$

where A (contact area)=19.625 mm^2 and x_0 and x_1 are the initial and maximum debonding displacements, respectively.

Gel Content (GC) and Crosslink Density (v_e)

The GC and v_e values of the SiPSA-T_x-C_y films were determined *via* equilibrium swelling in CH_2Cl_2.[34–36] Cylindrical specimens (20 mm diameter × 1 mm thickness) were weighed (m_{unex}, g), immersed in 20 mL of CH_2Cl_2 for 120 h with shaking, blotted dry, and re-weighed (m_s, g). After vacuum drying (45 °C, 12 h), the extracted mass (m_{ex}, g) was recorded. The GC and polymer volume fraction (v_e) were calculated using Eqs. (2) and (3), respectively:

$$\mathrm{GC}\ (\%) = \frac{m_{ex}}{m_{unex}} \times 100 \tag{2}$$

$$v = \frac{m_{ex}/\rho_p}{m_{ex}/\rho_p + (m_s - m_{ex})/\rho_p} \tag{3}$$

where ρ_s=1.33 g/cm^3 (CH_2Cl_2), and ρ_p=1.088 g/cm^3 (SiPSA). The average molecular weight between the crosslinks (M_c, g/mol) and v_e (mol/cm^3) was derived from the Flory-Rehner Eq. (4):[37]

$$v_e = \frac{\rho_p}{M_c} = -\frac{1}{V_s} \times \frac{\ln(1-v) + v + \chi v^2}{v^{1/3} - v/2} \tag{4}$$

where V_s is the molar volume of CH_2Cl_2 (64 cm^3/mol) and χ is the Flory-Huggins parameter for the polymer-solvent interaction (0.14).

Contact Angle and Solid Surface Free Energy (γ_S)

The static contact angles of water (θ_w) and diiodomethane (θ_{DIM}) on the SiPSA surface were measured using a goniometer (JC2000D6M, Zhongchen, China) with 50 μL of drops (n=10 measurements per sample, triplicate samples). γ_S ($\gamma_S = \gamma_S^D + \gamma_S^P$) was subsequently calculated using the Owens two-liquid method, according to Eq. (5):[38,39]

$$\gamma_L(1+\cos\theta) = 2\left(\gamma_S^D\gamma_L^D\right)^{1/2} + 2\left(\gamma_S^P\gamma_L^P\right)^{1/2} \tag{5}$$

where γ_S^D and γ_S^P represent the dispersive and polar components, respectively, γ_L ($\gamma_L = \gamma_L^D + \gamma_L^P$) is the surface energy of the liquid. However, γ_S^D and γ_S^P are both unknown; therefore, it is difficult to directly calculate γ_S using Eq. (5). Utilizing the established surface energy parameters of two test fluids for water (γ_L^D=21.8 mN/m, γ_L^P=51.0 mN/m) and diiodomethane (γ_L^D=48.5 mN/m, γ_L^P=2.3 mN/m), the γ_S^D and γ_S^P could be obtained.

Hydrolysis Stability

SiPSA strips (25.0 mm × 75.0 mm × 0.1 mm, initial mass m_0, g) were fully immersed in phosphate buffer saline (PBS, pH=7.4). At 15 min intervals, the specimens were removed from the solution, thoroughly dried, and weighed (mass at time t, m_t, g). The residual mass percentage (%) was calculated using Eq. (6):[40]

$$\text{Residual mass}\ (\%) = \frac{m_t}{m_0} \times 100 \tag{6}$$

Application Test

Cytotoxicity assay

Cytotoxicity against HeLa cells was evaluated using the MTT assay (details are provided in the electronic supplementary information, ESI).[17,41]

Direct peptide reactivity test (DPRA)

The DPRA was conducted in accordance with OECD Test Guideline 442C[42,43] (detailed protocol is available in Table S1 in ESI).

Skin irritation test

The skin irritation test was carried out according to ISO 10993-10 protocols (detailed protocol available in Fig. S1, Tables S2 and S3 in ESI).[43]

In vitro skin permeation study

The skin permeation study of DFS was conducted according to a previously reported method[44] (the detailed protocol is available in Table S4 in ESI).

Electrocardiogram (ECG) signal acquisition

ECG signals were acquired using a quasi-standard lead II configuration to ensure consistent monitoring of cardiac activity[43,45] (detailed protocol available in ESI).

All of the above data (adhesion performance, GC, v_e, contact angle, *etc.*) were tested three times, and the average value was used to calculate the error.

RESULTS AND DISCUSSION

Design and Structure Characterization of SiPSA

Fig. 1(a) depicts SiPSA, an innovative thermo-responsive skin-adhesive material fabricated by crosslinking PEG-Si with TMPTA. PEG-Si was synthesized *via* the aza-Michael addition between

PEGDA and APDS (Fig. S2 in ESI) following our established protocol.[31] In the synthesis of PEG-Si, PEGDA acts as an α,β-unsaturated carbonyl compound with an electron-deficient double bond. The amino groups in APDS possess a lone-pair of electrons that can attack this unsaturated bond, leading to an additional reaction. Owing to the inherent basicity of amino groups, the reaction proceeds readily at room temperature without any catalyst. After addition, a significant number of imino groups remain in PEG-Si, which can further undergo an aza-Michael addition with the unsaturated double bonds in TMPTA. This resulted in the cross-linking of PEG-Si and the formation of SiPSA. Successful PEG-Si synthesis was confirmed by FTIR (Fig. S3 in ESI), and ^{1}H-NMR spectra (Fig. S4 in ESI). The complete disappearance of the characteristic vinyl proton peaks (δ=5.88, 6.02, and 6.30 ppm) in the ^{1}H-NMR spectrum verified the full consumption of acrylate groups (detailed FTIR and NMR analyses are provided in ESI). The molecular weight of PEG-Si was approximately 9060 g/mol with a polydispersity of 1.23.

FTIR analysis of the SiPSA-$T_{0.75}$-$C_{0.5}$ hybrid (Fig. S5 in ESI) confirmed the successful integration of PEG-Si, TMPTA, and chitosan. Critically, the C=C bond absorption band (1627 cm^{-1}) of TMPTA[46] vanished. Concurrently, the characteristic chitosan —OH band (3446 cm^{-1})[47] remained, alongside intact PEG-Si group bonds, demonstrating successful reaction completion. Further confirmation was obtained from ^{1}H-NMR (Fig. S6 in ESI): signals for C=C double bonds at 6.18, 5.69 and 4.28 ppm (H11, H12, and H13, respectively) of TMPTA disappeared in SiPSA. New peaks emerged at 2.72 ppm (H11 and H13), indicating that a Michael addition reaction occurred. This NMR evidence confirmed that TMPTA functioned effectively as a crosslinking agent in SiPSA formation.

TMPTA Content-dependent Adhesive Performance of SiPSA

Fig. 2(a) systematically evaluates how TMPTA content influences the adhesive performance of SiPSA-T_x-$C_{0.5}$ (chitosan fixed at 0.5 wt%) on the skin. 180° peel strength measurements revealed a non-monotonic trend, and peaked at 211 N/m with 0.75 wt% TMPTA, then declined at higher concentrations. This trend reflects a critical balance between the cohesive and adhesive interactions. At low TMPTA (<0.5 wt%), insufficient crosslinking, indicated by low GC (<54.05%), low v_e (<1.80×10^{-6} mol/cm^3), and high M_c (>6.03×10^5 g/mol) (Table S5 in ESI), yields a viscoelastic fluid with negligible peel strength due to poor mechanical integrity. At optimal TMPTA (0.75 wt%), balanced crosslinking (GC=69.55%, v_e=1.88×10^{-6} mol/cm^3, M_c=5.78×10^5 g/mol) maximizes the interfacial adhesion while preserving the cohesive strength. At excessive TMPTA (≥1.0 wt%), over-crosslinking increases GC and v_e while decreasing M_c (GC≥ 82.30%, v_e≥4.73×10^{-6} mol/cm^3, M_c≤2.30×10^5 g/mol). This restricts chain mobility, diminishes wetting ability, and interfacial adhesion, even with enhanced cohesion.[48]

Probe tack tests further confirmed the non-monotonic trends for the maximum tack force and work of adhesion (W) with TMPTA content. Increasing TMPTA initially raised tack force and W, peaking at 0.75 wt% (tack force=2.3 N; W=67.4 J/m^2), then decreasing at higher loadings (Fig. 2a and Fig. S7

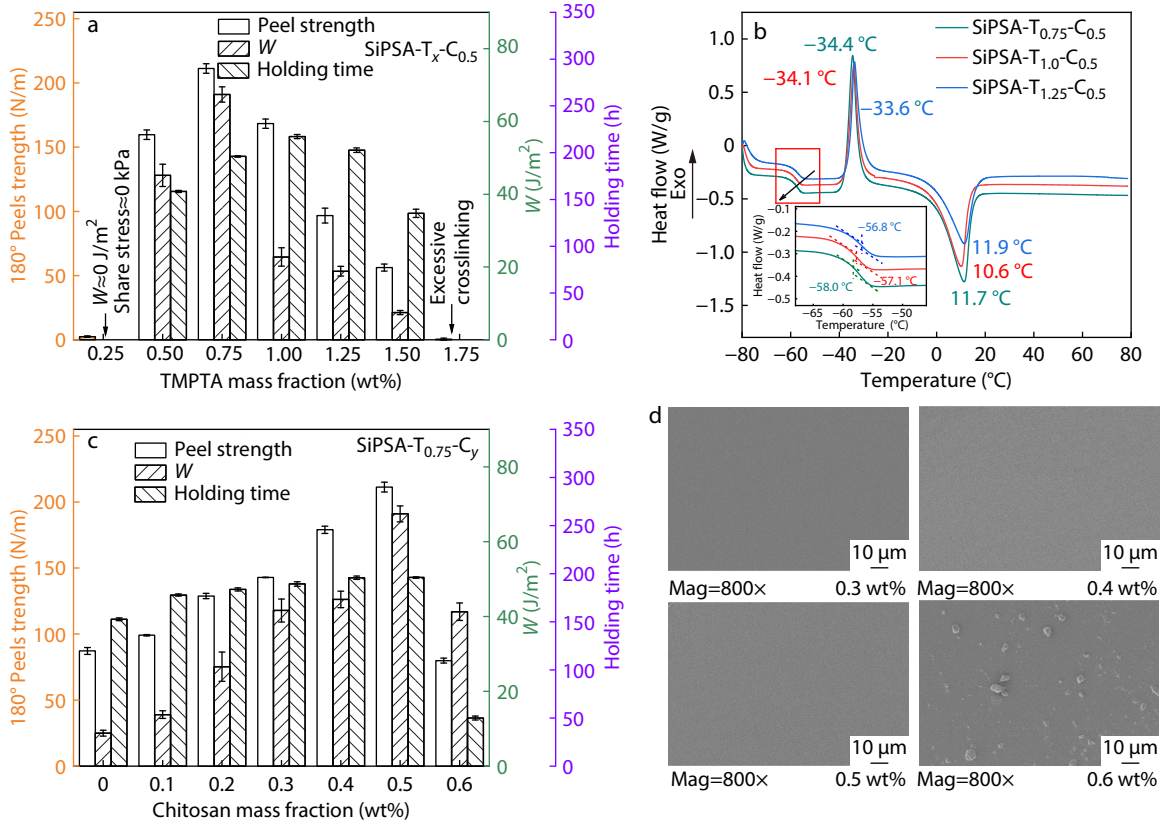

Fig. 2 (a) 180° Peel strength, work of adhesion (W), holding time and (b) the DSC spectra of SiPSA-T_x-$C_{0.5}$; (c) 180° Peel strength, W, holding time and (d) SEM images of SiPSA-$T_{0.75}$-C_y. Values are expressed as mean ± SD (n=3).

in ESI). These combined results identify 0.75 wt% TMPTA is optimal for adhesion performance, balancing the cohesive strength and interfacial energy dissipation. However, the holding time peaks at 1.0 wt% TMPTA (217 h) and then decreases with increasing TMPTA content. Mechanistically, a low TMPTA content limits cohesion, moderate TMPTA enhances cohesion without sacrificing wetting, and excessive TMPTA (>1.0 wt%) over-strengthens cohesion, reduces interfacial wettability, and causes the holding power to decline.

DSC analysis (Fig. 2b and Table S5 in ESI) demonstrated that the T_g of SiPSA-T_x-$C_{0.5}$ exhibited a marginal yet consistent increase with TMPTA content, range from −58.0 °C to −56.8 °C. This observation was attributed to the restricted segmental mobility induced by the elevated crosslink density (Table S5 in ESI), which stiffens the polymer network.[39] Notably, for SiPSA-$T_{0.75}$-$C_{0.5}$, distinct thermal transitions were identified, a crystallization exotherm (T_c) at −34.4 °C and a melting peak (T_m) at 11.7 °C, corresponding to the melting and crystallization domains of the SiPSAs matrix. Similar results were observed for SiPSA-$T_{1.0}$-$C_{0.5}$ and SiPSA-$T_{1.25}$-$C_{0.5}$ (Fig. 2b and Table S5 in ESI). These results indicated that moderate to high crosslink densities (≥0.75 wt% TMPTA) do not disrupt the inherent semi-crystalline structure of the SiPSA matrix, and that highlights the unique compatibility between crosslinking and crystallinity in these systems.

Surface wettability measurements further revealed critical insights into the interfacial behavior of SiPSAs. The water and diiodomethane contact angles (θ_w and θ_{DIM}, respectively) exhibited monotonic upward trends with increasing TMPTA content (Fig. S8 in ESI), whereas the total surface energy (γ_S) decreased correspondingly (Table S6 in ESI). This phenomenon is attributed to the enhanced surface hydrophobicity induced by the formation of a denser crosslinked network, which restricts the mobility of polar segments and reduces the surface polar interactions.[38] Importantly, measurements on the tested skin revealed a high γ_S (59.4 mN/m), emphasizing the significance of surface wettability in determining the interfacial adhesion. Notably, this reduction in directly correlates with the observed decline in adhesive performance at high crosslink densities because the mismatch between the low-energy SiPSA surface and high-energy skin impairs interfacial contact. Collectively, these thermal and surface characterization results underscore TMPTA concentration as a tunable parameter that governs the SiPSA microstructure (crosslink density and crystallinity) and surface properties (wettability), establishing a clear structure–performance relationship that innovatively guides the optimization of adhesive functionality for skin interfaces.

Chitosan Content-dependent Adhesive Performance of SiPSA

With the TMPTA content fixed at its optimal level (0.75 wt%), chitosan was introduced as a tackifier to fabricate the SiPSA-$T_{0.75}$-C_y series of adhesives. Measurements of the 180° peel strength, *W*, holding time, and tack force (Fig. 2c and Fig. S9 in ESI) revealed a non-monotonic dependence on chitosan loading, with peak values of 211 N/m, 67.4 J/m^2, 196 h, and 2.3 N, respectively, achieved at an optimal chitosan concentration of 0.5 wt% (SiPSA-$T_{0.75}$-$C_{0.5}$). Below this 0.5 wt% threshold, the obtained enhancement in the adhesive performance arises from two synergistic mechanisms. First, rich hydrophilic groups are helpful for improving the bonding performance between the adhesives and tissues.[49,50] The long chains of chitosan interpenetrate the SiPSA network, and the abundant —OH and —NH_2 groups present on chitosan introduce additional hydrogen-bonding sites, thereby strengthening the interfacial interactions between the PEG-Si network and contact surfaces (both skin and probe). Second, chitosan is hypothesized to penetrate the superficial layers of the skin, forming an entangled interface that further augments adhesion through mechanical interlocking,[51] as schematically illustrated in Fig. 1(b). Beyond 0.6 wt%, the miscibility limit of chitosan within the SiPSA network is exceeded, leading to chitosan precipitation and aggregation, which precipitates a sharp decline in adhesive properties. SEM images (Fig. 2d) confirmed the presence of segregated chitosan domains on the surface of the SiPSA matrix at higher loadings, directly validating this hypothesis.

Temperature-responsive Debonding Performance of SiPSA

SiPSA exhibits bidirectional thermal responsiveness (Fig. 1b), which distinguishes it from conventional single-mode thermoresponsive adhesives by enabling controlled adhesion modulation. Typically, temperature-controlled debonding of PSA involves two mechanisms: cohesive failure within the adhesive layer and interfacial failure at the substrate interface. Cohesive failure, which results in adhesive residue on the substrate, is generally undesirable. Interfacial failure can be achieved through two approaches: first, by altering the hydrophilicity/hydrophobicity of the adhesive molecules under thermal conditions to weaken the intermolecular interactions at the interface; and second, by enhancing the cohesive strength of the adhesive, increasing its elastic modulus, reducing its viscous modulus, and decreasing its wettability on the substrate to promote debonding.[52] Notably, the SiPSA developed in this study effectively achieves interfacial debonding under both high- and low-temperature conditions. At sub-ambient temperatures (<20 °C), the formation of a semicrystalline microstructure owing to PEG segments impairs interface wetting, facilitating clean, residue-free detachment.[16] Conversely, at hyperthermic temperatures (>40 °C), the thermally triggered hydrophilic-hydrophobic transition of PEG-Si diminishes skin biocompatibility, weakens interfacial adhesion.[31,41] This dual-mode mechanism ensures robust adhesion under physiological or ambient conditions (20–40 °C) while enabling on-demand release in dynamic thermal environments, a critical advance for adaptive wearable or biomedical applications.

To validate this mechanism, the optimal formulation, SiPSA-$T_{0.75}$-$C_{0.5}$ was selected for temperature-responsive debonding characterization. As shown in Fig. 3(a), the 180° peel strength of SiPSA-$T_{0.75}$-$C_{0.5}$ increases monotonically with bondline thickness, a trend consistent across debonding tests at 0 and 60 °C. This observation aligns with Keable's theoretical framework, which posits a direct proportionality between the peel strength and PSA layer thickness within the stable interfacial adhesive failure regime during high-speed peeling, a relationship further validated by experimental data.[53] To achieve robust adhesion (211 N/m at 37 °C) with efficient debonding (high- and low-temperature debonding rates of 72.70% at 60 °C and 82.54% at 0 °C, respectively), a 100 μm

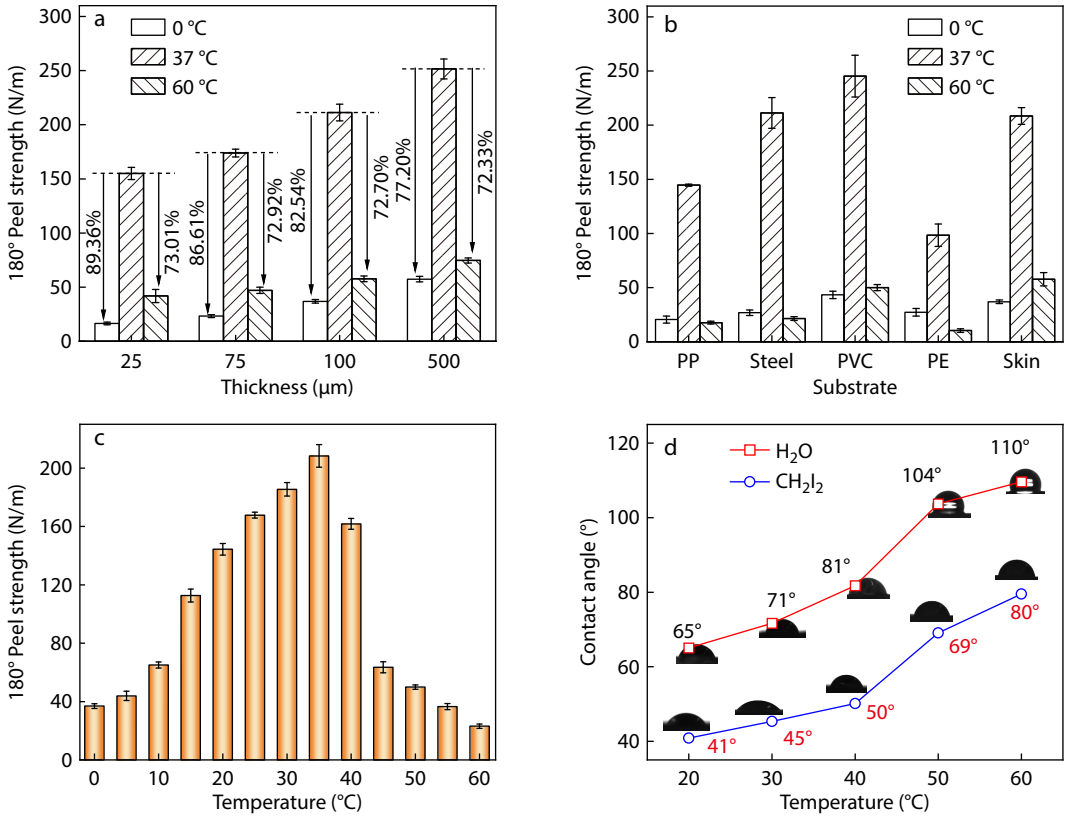

Fig. 3 Temperature-dependent adhesive performance of SiPSA-$T_{0.75}$-$C_{0.5}$: (a) 180° peel strength on skin for films of different thicknesses, (b) 180° peel strength on various substrates, (c) variation of 180° peel strength on skin with temperature; and (d) water and diiodomethane contact angle on SiPSA-$T_{0.75}$-$C_{0.5}$ as a function of temperature. Values are expressed as mean ± SD (n=3).

bondline thickness was chosen for subsequent analyses.

Temperature-controlled debonding PSAs have been extensively reported, typically achieving debonding either through cooling-induced crystallization (*e.g.*, DDPTA@ICE[16], P(TA-OA),[54] SA/TA-BAP[55]) or *via* heating (*e.g.*, BOC-protected acrylate PSA,[14] PP-HES[56]) (Table S7 in ESI). However, systems capable of debonding *via* both cooling and heating have rarely been reported. Moreover, the peel strength of SiPSA at room temperature reached 211 N/m, which is significantly higher than that of some reported temperature-controlled PSAs (*e.g.*, DDPTA@ICE: 33 N/m at 32 °C; P(TA-OA): 69 N/m at 33 °C; SA/TA-BAP: 46 N/m at 32 °C) (Table S7 in ESI).

Fig. 3(b) demonstrates the universal adhesive capability of SiPSA-$T_{0.75}$-$C_{0.5}$ across diverse substrates, including PP, PVC, steel, PE, and porcine skin. Notably, even on the low-surface-energy PE (Table S6 in ESI), the adhesive maintained a substantial 180° peel strength of 98 N/m at 37 °C. A clear inverse correlation emerged between the interfacial energy difference ($\Delta\gamma = |\gamma_{substrate} - \gamma_{SiPSA}|$) and peel strength: PVC (γ=41.5 mN/m, $\Delta\gamma$=7.6 mN/m, strength=245 N/m), steel (γ=59.8 mN/m, $\Delta\gamma$=10.7 mN/m, strength=208 N/m), skin (γ=59.4 mN/m, $\Delta\gamma$=10.3 mN/m, strength=211 N/m), PP (γ=36.6 mN/m, $\Delta\gamma$=12.5 mN/m, strength=144 N/m), and PE (γ=33.4 mN/m, $\Delta\gamma$=15.7 mN/m, strength=98 N/m). Importantly, this temperature-responsive debonding behavior was consistent across all substrates, with peel strength significantly reduced at 0 and 60 °C relative to ambient conditions, confirming the mechanism's universality.

The temperature-dependent peel strength of SiPSA-$T_{0.75}$-$C_{0.5}$ (37 °C baseline) across 0–60 °C (Fig. 3c) further validated its adaptive performance. Within the physiologically relevant range (25–40 °C), peel strength remained robust adhesion (>145 N/m), peaking at 208 N/m at 35 °C, confirming stability for biomedical applications. Below 10 °C, peel strength declined sharply, attributable to PEG segment crystallization within the crosslinked network. This evidenced by an exothermic DSC peak at about −34 °C, a crystal melting peak at around 11 °C (Fig. 2b), and X-ray diffraction (XRD) peaks at 2θ≈10° and 2θ≈20° at 0 °C (Fig. S10a in ESI). This crystallization induced a transparent-to-opaque transition (visible light transmittance: 97% at 37 °C versus 20% at 0 °C; Fig. S10b in ESI), forming a rigid semicrystalline structure that compromises wetting. Conversely, at 45–60 °C, peel strength deteriorated due to a hydrophilic-hydrophobic transition, as indicated by a marked increase in water contact angle (θ_w: 65°→110°; Fig. 3d) and decrease in surface energy (γ: 49.12→18.15 mN/m, Table S8 in ESI), directly correlating with interfacial adhesive failure. Collectively, DSC, XRD, and wetting measurements establish a rigorous structure-property relationship, linking temperature-induced morphological transitions (crystallization at low temperature, hydrophobicity at high temperature) to adaptive adhesive performance modulation.

Dynamic rheological analysis characterized the viscoelastic properties of SiPSA-$T_{0.75}$-$C_{0.5}$, revealing key parameters, including the storage modulus (E'), loss modulus (E''), and loss tangent (tanδ) (Fig. S11 in ESI). Significantly, the T_g of −30 °C

determined by rheological methods represents a substantial 28 °C depression compared to values obtained *via* DSC. This discrepancy arises from inherent differences between the two techniques.[57] Critically, this lower T_g is functionally essential, as it facilitates energy dissipation mechanisms and interfacial wetting behavior fundamental to effective PSA performance. The pronounced rheological softening occurring below the DSC-determined T_g directly underpins the pressure-sensitive characteristics of the material, establishing an optimal balance between the cohesive integrity and adhesive tack at application temperatures.

TGA analysis (Fig. S12 in ESI) demonstrates significant thermal stability, and thermal decomposition occurs in distinct stages: a major weight loss centered at 154.84 °C is related to reversible dissociative *β*-aminoamide dynamic exchange into acrylamides and amines[58,59] and chitosan degradation; a major event at 296.33 °C is assigned to PEG segment degradation;[60] and decomposition of Si—O—Si component culminates 470.18 °C.

Potential Clinical and Bio-electronic Applications

Achieving bonding with water in an environment has always been challenging.[61] SiPSA-$T_{0.75}$-$C_{0.5}$ exhibited a significant water absorption capacity, as demonstrated by the rapid and uniform uptake of rhodamine B solution from stained agar, leaving no residue on dry paper after removal (Fig. S13 in ESI). Capillary-driven transport was further evidenced by the unidirectional wicking of the rhodamine B solution through the film matrix (Fig. S14 in ESI). The intrinsic hydrophilicity contrasts sharply with the behavior of conventional PSAs, which typically lack water-absorbing functionality (control film, Fig. S13 in ESI).

Critically, SiPSA maintained effective interfacial adhesion despite hydration. Remarkably, SiPSA-$T_{0.75}$-$C_{0.5}$ maintained robust peel strength (>160 N/m on the skin) even after swelling to 20 vol% water uptake (Fig. 4a). Time-dependent static θ_w measurements on SiPSA-T_x-$C_{0.5}$ reveal substantial decreases within 30 s across all formulations (Fig. 4b). This dynamic wetting behavior stems from the unique surface architecture, the siloxane-enriched hydrophobic barrier initially repels water, while enabling rapid diffusion into the polymer matrix. The absorbed water molecules subsequently form hydrogen bonds with carbonyl groups, immobilizing within the matrix and preserving a tacky, dry external surface (Fig. 4c). This mechanism sustains strong interfacial adhesion, which is critical for performance in moist environments.[62] Furthermore,

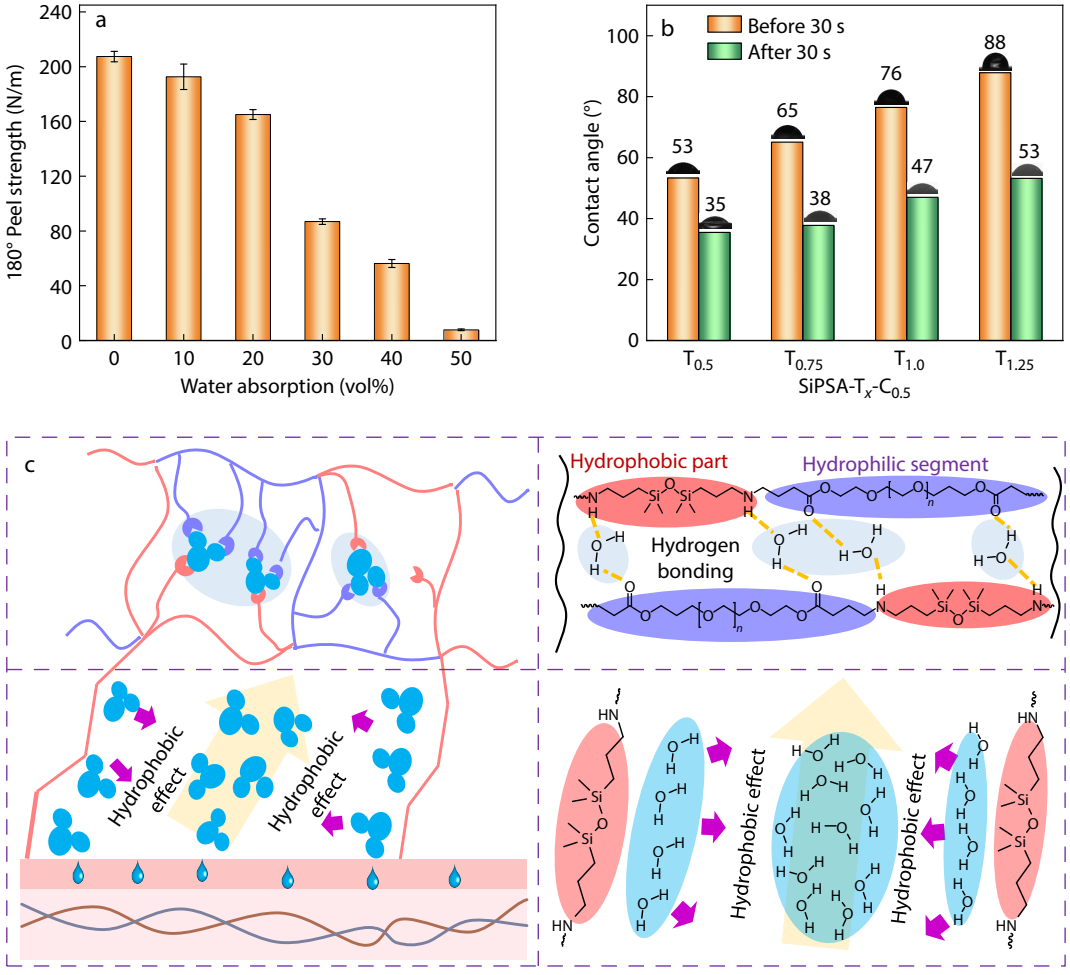

Fig. 4 (a) The 180° peel strength along with the variation of water absorption of SiPSA-$T_{0.75}$-$C_{0.5}$; (b) The changes in contact angles of water droplets on SiPSA-T_x-$C_{0.5}$ before and after being placed for 30 s; (c) Schematic diagram of the water absorption mechanism of SiPSA. Values are expressed as mean ± SD (n=3).

https://doi.org/10.1007/s10118-026-3766-7

hydrolytic degradation studies in PBS confirmed the capacity of SiPSA for controlled breakdown under aqueous conditions (Fig. S15 in ESI).

Collectively, these properties, including targeted water absorption without surface tack loss, sustained adhesion strength when hydrated, and programmable hydrolytic dissolution, establish SiPSA as an innovative platform for reliable temporary adhesion to hydrated biological substrates including tissue wounds and moist skin.

SiPSA demonstrated exceptional biocompatibility (Fig. 5a) and a controlled hydrolytic degradation profile, ensuring minimal risk to the surrounding tissue upon application. SiPSA exhibits an exceptionally low skin sensitization potential. This is evidenced by the direct peptide reactivity assay (DPRA) showing minimal depletion of cysteine (2.2%±0.46%) (Fig. S16a and Table S9 in ESI) and lysine (1.62%±0.69%) (Fig. S16b and Table S10 in ESI), thus meeting the stringent safety requirements for transdermal delivery systems. In the single-exposure dermal irritation study, the test animals were evaluated for erythema and edema at 1, 24, 48, and 72 h post-application (Fig. S17 and Tables S11 and S12 in ESI) using the Draize criteria. The SiPSA-treated sites exhibited no edema and only negligible erythema, with mean daily scores of 0 and 0.3, respectively. These values were comparable to those of the negative control and markedly lower than those of the positive control, demonstrating negligible skin irritation caused by SiPSA.

Critically, SiPSA-$T_{0.75}$-$C_{0.5}$ offers excellent 180° peel strength (211 N/m) along with efficient debonding at 0 and 60 °C compared to three commercial plasters (Sunflower Pharmaceuti-

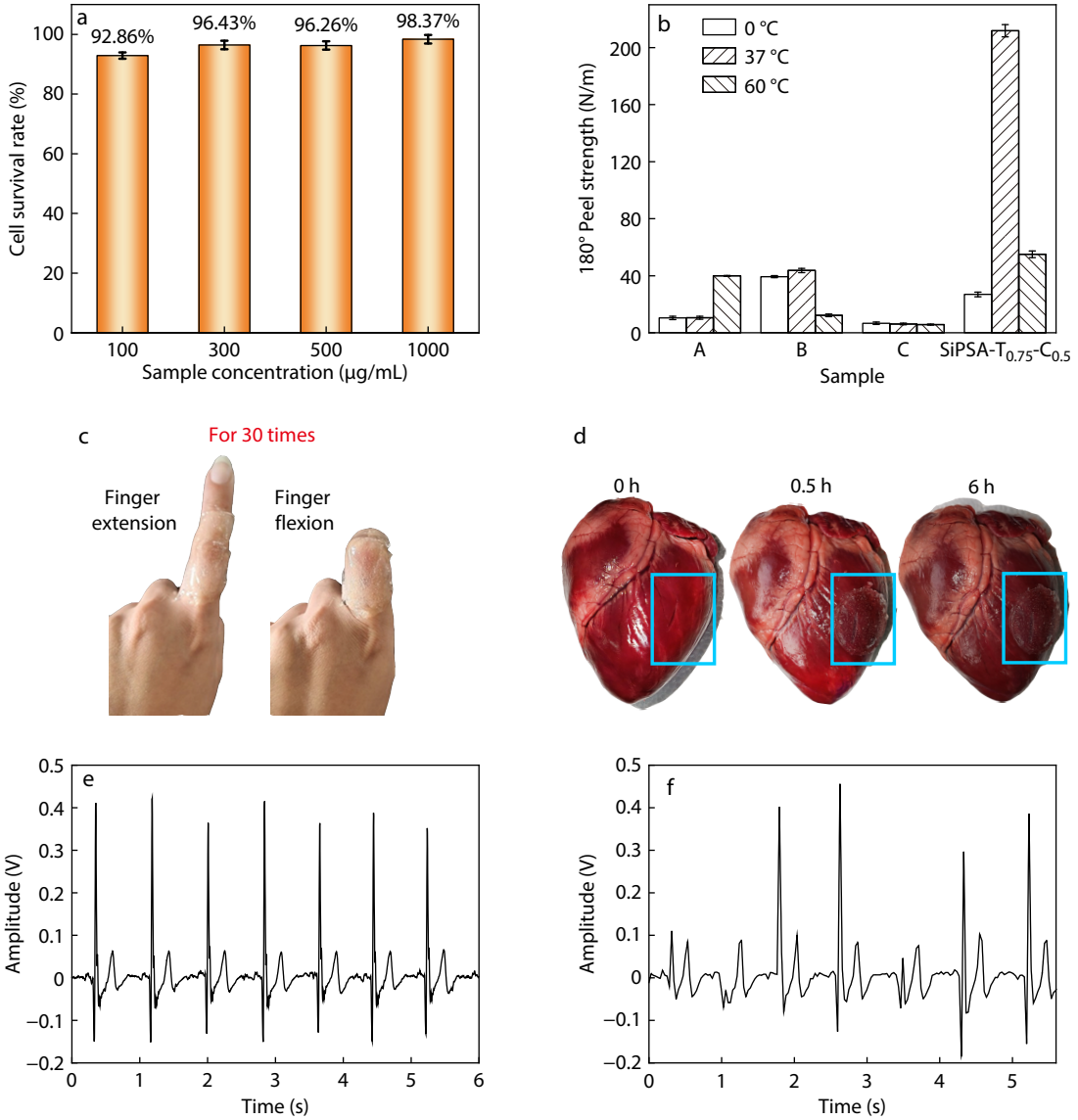

Fig. 5 (a) The survival rate of HeLa cells in different concentrations of SiPSA-$T_{0.75}$-$C_{0.5}$ solution; (b) 180° Peel strength of SiPSA-$T_{0.75}$-$C_{0.5}$ benchmarked against three commercial topical adhesive patch (A: Sunflower Pharmaceutical, B: Musk Bone Strengthening Granules, and C: Hisamitsu Pharmaceutical); (c) The adhesive film is affixed to a mobile joint (finger) and subjected to 30 consecutive flexion–extension cycles; (d) The adhesive film is applied to a cardiac wound and holding for 6 h; (e) Electrocardiograms recorded during rest and (f) during physical activity. Values are expressed as mean ± SD (n=3).

https://doi.org/10.1007/s10118-026-3766-7

cal, Musk Bone Strengthening Granules, and Hisamitsu Pharmaceutical, Fig. 5b). Furthermore, SiPSA maintained exceptional flexibility and resisted delamination through 30 repeated joint flexion cycles (Fig. 5c). This combination of strong adhesive strength, intrinsic degradability, and biocompatibility enables novel applications, including secure closure of internal tissue wounds without the need for post-healing removal, and reliable attachment of ECG sensors that withstand exercise-induced sweating for sensitive cardiac monitoring (Figs. 5d–5f).

The robust skin adhesion of SiPSA renders it particularly advantageous for transdermal drug delivery. As a representative example, the anti-inflammatory and analgesic agent DFS was evaluated under equivalent drug loading of 85.23 mg/cm^3. Remarkably, the 24 h transdermal permeation rate reached 78.33% (Table S13 in ESI), which was significantly higher than that achieved with conventional carrier systems (Fig. S18 in ESI).

A key innovative feature is the dual-temperature release mechanism triggered by either elevated or reduced temperatures. This unique property, coupled with moderate hydrolytic degradation and robust performance on moist substrates, establishes SiPSA-$T_{0.75}$-$C_{0.5}$ as a versatile platform that is ideally suited for emergency interventions on wet skin and open wounds, allowing clinicians to tailor removal strategies to specific clinical scenarios.

CONCLUSIONS

This study establishes SiPSA as a multifunctional adhesive platform that exhibits dual-temperature-triggered debonding, robust adhesion on wet biological surfaces, and controlled hydrolytic degradation. Optimized crosslinking yields exceptional adhesive strength (211 N/m) on skin at physiological temperature (37 °C), while enabling rapid, on-demand release through thermal stimuli. Heating to 60 °C induces a dramatic 72.7% reduction in adhesion, and cooling to 0 °C triggers an even more significant 82.5% reduction. Critically, the material maintains this strong interfacial bonding despite absorbing saline solution equivalent to 20% of its volume, which is a remarkable fluid uptake capacity that outperforms conventional medical adhesives prone to failure in moist environments. Combined with its demonstrated biocompatibility and strong adhesion to hydrated tissues, SiPSA may be suitable for use in scenarios that require dependable attachment to dynamic or moist physiological environments. This includes applications such as emergency wound closure on wet skin, temperature-responsive removal of medical devices, and advanced bio-adhesive interfaces for tissue repair, among other possible uses.

Conflict of Interests

The authors declare no interest conflict.

Electronic Supplementary Information

Electronic supplementary information (ESI) is available free of charge in the online version of this article at http://doi.org/10.1007/s10118-026-3766-7.

Data Availability Statement

The data supporting the findings of this study are available from the corresponding author upon reasonable request.

ACKNOWLEDGMENTS

This work was financially supported by the Nature Science Foundation of Shandong Province, China (Nos. ZR2022MB051 and ZR2021MB112), Postdoctoral Science Foundation of China (No. 2022M712343), Jinan City University Integration Development Strategy Project (No. JNSX2024030), Key Laboratory of Special Functional Aggregates of Ministry of Education, Shandong University (No. JJT-2023-02), and Shandong SD-Link New Material Technology Co., Ltd.

REFERENCES

1 Fitzgerald, D. M.; Colson, Y. L.; Grinstaff, M. W. Synthetic pressure sensitive adhesives for biomedical applications. *Prog. Polym. Sci.* **2023**, *142*, 101692.
2 Swanson, S.; Bashmail, R.; Fellin, C.; Luu, V.; Shires, N.; Cox, P.; Nelson, A.; MacKenzie, D.; Taroc, A. M.; Nelson, L.; Seibel, E. Prototype development of a temperature-sensitive high-adhesion medical tape to reduce medical-adhesive-related skin injury and improve quality of care. *Int. J. Mol. Sci.* **2022**, *23*, 7164.
3 Gohl, J. A.; Zummo, W. H.; Jennings, R. M.; Defante, A. P.; Davis, C. S. Deformation of soft substrates during adhesive peel testing. *J. Polym. Sci.* **2024**, *62*, 3830–3838.
4 Gong, K.; Sun, P.; Cai, Y.; Wang, X.; Pang, Y.; Liu, C.; Guo, J.; Fang, L. Water-compatible cross-linked pyrrolidone acrylate pressure-sensitive adhesives with persistent adhesion for transdermal delivery: Synergistic effect of hydrogen bonding and electrostatic force. *Acta Biomater.* **2024**, *179*, 130–148.
5 Tan, X.; Hu, X.; Pan, X.; Xie, W.; Li, D.; Yuan, Y.; Wang, J. An integrated Janus patch with asymmetric tissue adhesion for enhanced postoperative adhesion prevention. *Polym. Sci. Technol.* **2025**, *1*, 120–131.
6 Ranji, S.; Qin, P.; Lee, M. C. Synergistic effects of various hollow particles on mechanical and adhesive properties of impact protection film. *J. Polym. Res.* **2025**, *32*, 170.
7 Pradeep, S. V.; Kandasubramanian, B.; Sidharth, S. A review on recent trends in bio-based pressure sensitive adhesives. *J. Adhesion* **2023**, *99*, 2145–2166.
8 Hu, X.; Zhang, Z.; Chen, G.; Hou, P.; Zhang, Q.; Zhang, D.; Liu, X.; Zhang, L. Enhanced underwater adhesion of chitooligosaccharide-based pressure-sensitive adhesives and their potential in wound healing applications. *Carbohyd. Polym.* **2025**, *368*, 124227.
9 Mozelewska, K.; Antosik, A. K. Influence of silicone additives on the properties of pressure-sensitive adhesives. *Materials* **2022**, *15*, 5713.
10 Montemayor, M. D.; Iverson, E. T.; Dahle, L. R.; Green, A.; Tenorio, E.; Moran, A. V.; Rodriguez-Melendez, D.; Chang, E.; Karim, M. J.; Haridas, B.; Grunlan, J. C. Polyelectrolyte complex coacervate adhesive for wearable medical devices. *Macromol. Rapid Comm.* **2025**, *46*, 2500117.
11 Robertson, F.; Wang, Y.; Rosing, H. An oligomeric switch that rapidly decreases the peel strength of a pressure-sensitive adhesive. *Int. J. Adhes. Adhes.* **2014**, *55*, 64–68.

Graphical Abstract

Moisture-resistant and Thermally Dual-detachable Silicone-contained Pressure-sensitive Adhesive: Preparation and Potential Applications in Medical Care

Feng-Ming Yin, Xiao-Xia Zhou, Hai-Chao Yu, Shu-Sheng Li, Zhi-Qiu Ye, Xu-Bao Jiang, Xiao-Li Zhu, Sheng-Yu Feng, and Xiang-Zheng Kong

University of Jinan; Shandong University

This study introduces a silicone-contained pressure-sensitive adhesive synthesized by crosslinking thermo-responsive poly(ethylene glycol-*co*-siloxane) with trimethylol-propane triacrylate and a chitosan tackifier. This adhesive offers strong skin adhesion at 37 °C and enables on-demand, rapid detachment by either heating to 60 °C or cooling to 0 °C.

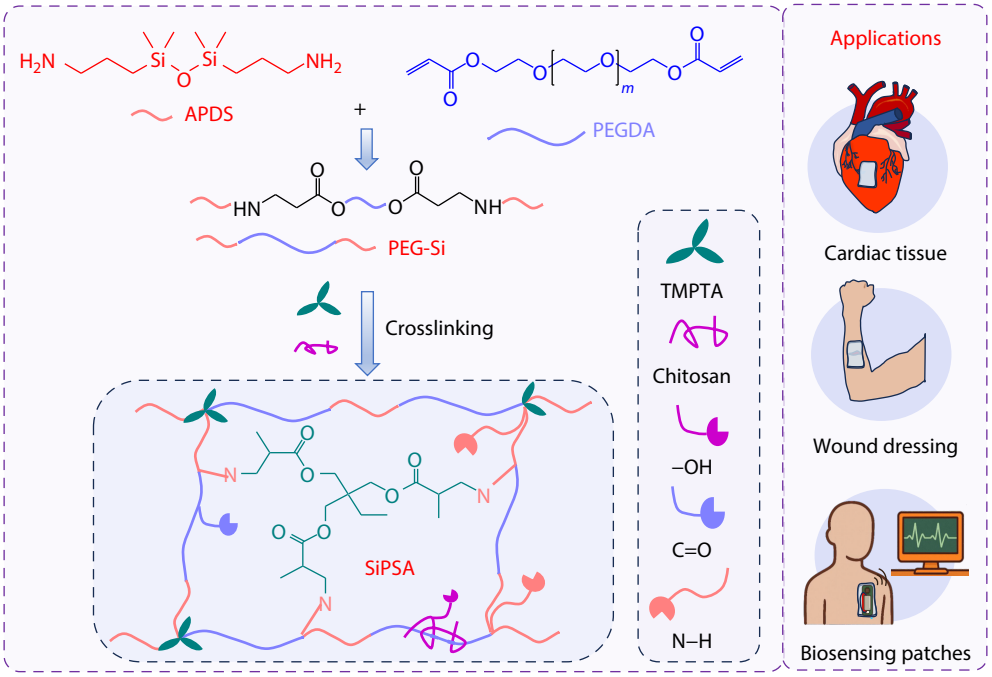

Chinese J. Polym. Sci. 2026 *https://doi.org/10.1007/s10118-026-3766-7*

12 Lou, P.; Li, X.; Yao, M.; Nie, J.; He, Y. Thermal debonding pressure-sensitive adhesive blended with liquid crystal polymers. *Prog. Org. Coat.* **2023**, *185*, 107932.
13 Bandl, C.; Kern, W.; Schlögl, S. Adhesives for "debonding-on-demand": Triggered release mechanisms and typical applications. *Int. J. Adhes. Adhes.* **2020**, *99*, 102585.
14 Sakamoto, T.; Suzuki, Y.; Matsumoto, A. Precise control of thermal deprotection behavior and dismantlable adhesion property of the acrylate copolymers containing BOC-protected hydroxy group. *Polymer* **2022**, *262*, 125416.
15 Hwang, J.; Lim, D.; Lee, G.; Kim, Y. E.; Park, J.; Baek, M. J.; Kim, H. S.; Park, K.; Ku, K. H.; Lee, D. W. Ambient air-operated thermo-switchable adhesion of *N*-isopropylacrylamide-incorporated pressure sensitive adhesives. *Mater. Horiz.* **2023**, *10*, 2013–2023.
16 Zeng, Q.; Wang, F.; Hu, R.; Ding, X.; Lu, Y.; Shi, G.; Haick, H.; Zhang, M. Debonding-on-demand polymeric wound patches for minimal adhesion and clinical communication. *Adv. Sci.* **2022**, *9*, 2202635.
17 Li, X. D.; Li, S. S.; Jiang, X. B.; Zhu, X. L.; Kong, X. Z. Unconventional fluorescent and multi-responsive polysiloxane: Synthesis, characterization and biological applications. *Chinese J. Polym. Sci.* **2024**, *42*, 579–590.
18 Guo, R.; Qi, W.; Liu, H.; Li, D.; Chen, G.; Li, Q.; Zhou, Z. Dynamic borate ester bond-based 3D printing fluorescence polysiloxane with self-healing, antimicrobial, and shape memory. *Chem. Eng. J.* **2024**, *485*, 149850.
19 Xiang, Z.; Gao, C.; Long, T.; Ding, L.; Zhou, T.; Wu, Z. Force-field benchmark for polydimethylsiloxane: Density, heat capacity, isothermal compressibility, viscosity and thermal conductivity. *J. Phys. Chem. B* **2025**, *129*, 1864–1873.
20 Zhang, H.; Guo, Y.; Zhang, S.; Yu, B.; Li, X.; Ning, N.; Tian, H.; Tian, M. Sustainable and cytocompatible thermoplastic vulcanizate based on silicone rubber and polycaprolactone. *Ind. Eng. Chem. Res.* **2025**, *64*, 11952–11960.
21 Karimi Nikoo, K.; Dvornic, P. R.; Self, J. L.; Long, T. E. Siloxane-containing polymers: From synthesis and characterization to

advanced applications and sustainability. *Polym. Int.* **2025**, *74*, 633–650.
22 Yu, M. M.; Li, J.; Chen, Y. H.; Zhang, Q. Y. Reprocessable form-stable phase change materials with high latent heat via dynamically cross-linked polysiloxane networks for efficient thermal energy storage. *J. Energy Storage* **2025**, *131*, 115866.
23 Fischer, S. C. L.; Kruttwig, K.; Bandmann, V.; Hensel, R.; Arzt, E. Adhesion and cellular compatibility of silicone-based skin adhesives. *Macromol. Mater. Eng.* **2017**, *302*, 1600526.
24 Antosik, A. K.; Mozelewska, K.; Piątek-Hnat, M.; Czech, Z.; Bartkowiak, M. Silicone pressure-sensitive adhesives with increased thermal resistance. *J. Therm. Anal. Calorim.* **2022**, *147*, 7719–7727.
25 Zeng, Y.; Xia, J. UV-cured silicone pressure-sensitive adhesive with adjustable adhesion and viscoelastic properties via thiol-ene chemistry. *Prog. Org. Coat.* **2024**, *194*, 108545.
26 Antosik, A. K.; Musik, M.; Miądlicki, P.; Weisbrodt, M.; Wilpiszewska, K. Influence of acid-modified clinoptilolite on the self-adhesive properties of silicone pressure-sensitive adhesives. *Polymers* **2023**, *15*, 707.
27 Antosik, A. K.; Gziut, K.; Weisbrodt, M.; Bartkowiak, M.; Kowalczyk, A. The effect of Pt-type catalysts on self-adhesive properties of silicone pressure-sensitive adhesives. *Silicon* **2024**, *16*, 1611–1618.
28 Zhou, Y.; Zhao, Z.; Liu, Z.; Chen, H.; Yan, H.; Tan, J.; Li, F. UV-curable silicone pressure-sensitive adhesive based on thiol-ene reaction. *Prog. Org. Coat.* **2024**, *186*, 107954.
29 Zhang, W.; Wang, R.; Yang, Z.; Bai, Y.; Meng, L.; Wang, Y. Synthesis of UV rapid curing silicone coatings via photoinitiated thiol-ene click polymerization for pressure-sensitive adhesive. *Polymer* **2023**, *283*, 126222.
30 Boyadzhieva, S.; Sorg, K.; Danner, M.; Fischer, S. C. L.; Hensel, R.; Schick, B.; Wenzel, G.; Arzt, E.; Kruttwig, K. A self-adhesive elastomeric wound scaffold for sensitive adhesion to tissue. *Polymers* **2019**, *11*, 942.
31 Li, L.; Li, S.; Cui, H.; Zhu, X.; Kong, X. Z. Phase transition and fluorescence emission of multiresponsive poly(ethylene glycol-*co*-siloxane) and its application for uric acid detection. *ACS Appl. Polym. Mater.* **2023**, *5*, 9413–9424.
32 Takahashi, K.; Yamada, M.; Sasaki, T.; Nakamura, T. Viscous dissipative energy density as a general adhesion characteristic of adhesive tape. *Soft Matter* **2025**, *21*, 6078–6087.
33 Zhang, P.; Zhang, B.; Pan, J.; Zhang, G.; Ma, C.; Zhang, G. Ultrastrong and versatile nonisocyanate polyurethane adhesive under extreme conditions. *Chem. Mater.* **2023**, *35*, 7730–7740.
34 Zhuang, M.; Wang, Y.; Xu, Y.; Jiang, J.; Xu, H.; Li, Y.; Li, G.; Xi, K. Construction and properties of release coating based on hydrogen-terminated hyperbranched polysiloxane. *Prog. Org. Coat.* **2025**, *200*, 108968.
35 Panchireddy, S.; Grignard, B.; Thomassin, J. M.; Jerome, C.; Detrembleur, C. Catechol containing polyhydroxyurethanes as high-performance coatings and adhesives. *ACS Sustainable Chem. Eng.* **2018**, *6*, 14936–14944.
36 Guo, B.; Chen, F.; Lei, Y.; Liu, X.; Wan, J.; Jia, D. Styrene-butadiene rubber/halloysite nanotubes nano- composites modified by sorbic acid. *Appl. Surf. Sci.* **2009**, *255*, 7329–7336.
37 Xu, S.; Zhang, Y.; Wang, M.; Zhao, H.; Hu, W. Comparative study on determination methods of crosslinking density of silicone rubber. *China Rubber Ind.* **2017**, *64*, 624–626.
38 Xu, C.; Chen, G.; Tan, Z.; Hu, Z.; Qu, Z.; Zhang, Q.; Lu, M.; Wu, K.; Lu, M.; Liang, L. Evaluation of cytotoxicity in vitro and properties of polysiloxane-based polyurethane/lignin elastomers. *React. Funct. Polym.* **2020**, *149*, 104514.
39 Xu, C. A.; Qu, Z.; Lu, M.; Meng, H.; Zhan, Y.; Chen, B.; Wu, K.; Shi, J. Effect of rosin on the antibacterial activity against *S. aureus* and adhesion properties of UV-curable polyurethane/polysiloxane pressure-sensitive adhesive. *Colloid Surface A* **2021**, *614*, 126146.
40 Fang, R.; Yu, N.; Chen, S.; Xu, X.; Zhang, J. Hemoadhican-based self-leveling Janus patch for comprehensive prevention of postoperative adhesions. *Mater. Today Bio* **2025**, *33*, 102021.
41 Yin, F. M.; Wu, L. L.; Li, S. S.; Pan, X. N.; Zhu, X. L.; Jiang, X. B.; Kong, X. Z. Unconventional fluorescent and multi-responsive polyethyleneimine with LCST and UCST behavior: Synthesis, characterization and biological applications. *Chinese J. Polym. Sci.* **2024**, *42*, 826–837.
42 Marcelis, Q.; Deconinck, E.; Rogiers, V.; Vanhaecke, T.; Desmedt, B. Applicability of the DPRA on mixture testing: Challenges and opportunities. *Arch. Toxicol.* **2023**, *97*, 2453–2461.
43 Xie, C.; Li, L. Y.; Li, S. S.; Zong, C. Y.; Jiang, X. B.; Zhu, X. L.; Feng, S. Y.; Kong, X. Z. Poly(hydroxy urethane-siloxane) pressure-sensitive adhesive: Synthesis, characterization and its usage for skin-contact sensors. *Chinese J. Polym. Sci.* **2026**, *44*, 536–548.
44 Iliopoulos, F.; Goh, C. F.; Haque, T.; Rahma, A.; Lane, M. E. Dermal delivery of diclofenac sodium-*in vitro* and *in vivo* studies. *Pharmaceutics* **2022**, *14*, 2106.
45 Lee, B. K.; Ryu, J. H.; Baek, I. B.; Kim, Y.; Jang, W. I.; Kim, S. H.; Yoon, Y. S.; Kim, S. H.; Hong, S. G.; Byun, S.; Yu, H. Y. Silicone-based adhesives with highly tunable adhesion force for skin-contact applications. *Adv. Healthc. Mater.* **2017**, *6*, 1700621.
46 Wang, S. C.; Chen, P. C.; Hwang, J. Z.; Huang, C. Y.; Yeh, J. T.; Chen, K. N. A new tri-functional azetidine compound for self-curing aqueous-based PU system. *J. Appl. Polym. Sci.* **2012**, *124*, 175–181.
47 Chen, S. H.; Tsao, C. T.; Chang, C. H.; Wu, Y. M.; Liu, Z. W.; Lin, C. P.; Wang, C. K.; Hsieh, K. H. Synthesis and characterization of thermal-responsive chitin-based polyurethane copolymer as a smart material. *Carbohyd. Polym.* **2012**, *88*, 1483–1487.
48 Jin, K.; López Barreiro, D.; Martin-Martinez, F. J.; Qin, Z.; Hamm, M.; Paul, C. W.; Buehler, M. J. Improving the performance of pressure sensitive adhesives by tuning the crosslinking density and locations. *Polymer* **2018**, *154*, 164–171.
49 Zhang, Y.; Liu, Y.; Liu, Y.; Zuo, P.; Miao, S.; Hu, B.; Kang, Y.; Liu, W.; Yang, Q.; Ren, H.; Yang, P. α-Helix-mediated protein adhesion. *J. Am. Chem. Soc.* **2023**, *145*, 17125–17135.
50 Bai, J. W.; Liu, W.; Wen, B.; Lei, Z. L.; Li, C.; Ren, H.; Yang, P. Synergistic functional group interactions for stable interfacial adhesion: Insights from amyloid- inspired polymers. *Chinese J. Polym. Sci.* **2025**, *43*, 1096–1104.
51 Cintron-Cruz, J. A.; Freedman, B. R.; Lee, M.; Johnson, C.; Ijaz, H.; Mooney, D. J. Rapid ultratough topological tissue adhesives. *Adv. Mater.* **2022**, *34*, 2205567.
52 Blelloch, N. D.; Yarbrough, H. J.; Mirica, K. A. Stimuli-responsive temporary adhesives: Enabling debonding on demand through strategic molecular design. *Chem. Sci.* **2021**, *12*, 15183–15205.
53 Poh, B. T.; Lamaming, J. Effect of testing rate on adhesion properties of acrylonitrile-butadiene rubber/standard malaysian rubber blend-based pressure-sensitive adhesive. *J. Coat.* **2013**, *2013*, 519416.
54 Zheng, Y.; Wu, M.; Duan, M.; Jin, Q.; Chen, S.; Wang, X.; Zhou, D. Skin temperature-triggered switchable adhesive coatings for wearing comfortable epidermal electronics. *Chem. Eng. J.* **2024**, *488*, 150459.
55 Gao, M.; Wu, H.; Plamthottam, R.; Xie, Z.; Liu, Y.; Hu, J.; Wu, S.; Wu, L.; He, X.; Pei, Q. Skin temperature- triggered, debonding-on-demand sticker for a self-powered mechanosensitive communication system. *Matter* **2021**, *4*, 1962–1974.
56 Sato, E.; Yuri, M.; Fujii, S.; Nishiyama, T.; Nakamura, Y.; Horibe, H. Liquid marble containing degradable polyperoxides for adhesion force-changeable pressure- sensitive adhesives. *RSC Adv.* **2016**, *6*, 56475–56481.

57 Koshimizu, N.; Saed, M. O. Switchable pressure-sensitive adhesion in nematic side-chain liquid crystal elastomers. *Macromolecules* **2025**, *58*, 12191−12200.
58 Tian, W.; He, E.; Yang, Z.; Wang, Y.; Zhang, S.; Wei, Y.; Niu, K.; Liang, H.; Ji, Y. β-Amino ester-based dynamic epoxy adhesive with high impact and cryogenic tolerance. *Chem. Eng. J.* **2026**, *530*, 173452.
59 Portone, F.; Nguyen, L. T.; Pinalli, R.; Pedrini, A.; Du Prez, F. E.; Dalcanale, E. Debondable phenoxy-based structural adhesives with β-amino amide containing reversible crosslinkers. *RSC Appl. Polym.* **2025**, *3*, 637−642.
60 Wang, Y.; Yu, X.; Zhang, H.; Fan, X.; Zhang, Y.; Li, Z.; Miao, Y. E.; Zhang, X.; Liu, T. Highly stretchable, soft, low-hysteresis, and self-healable ionic conductive elastomers enabled by long, functional cross-linkers. *Macromolecules* **2022**, *55*, 7845−7855.
61 Lu, S. Y.; Zhang, R. Y.; Gao, W. T.; Zhang, D.; Zhang, X. P.; Li, C. H. An underwater self-healing polysulfide elastomer with in-situ curing and adhesion. *Polym. Sci. Technol.* **2025**, *1*, 458−467.
62 Yuk, H.; Varela, C. E.; Nabzdyk, C. S.; Mao, X.; Padera, R. F.; Roche, E. T.; Zhao, X. Dry double-sided tape for adhesion of wet tissues and devices. *Nature* **2019**, *575*, 169−174.

https://doi.org/10.1007/s10118-026-3766-7